

Research Article

Zhong Wang, Kesu Cai, Yang Lu, Haining Wu, Yuee Li*, and Qingguo Zhou*

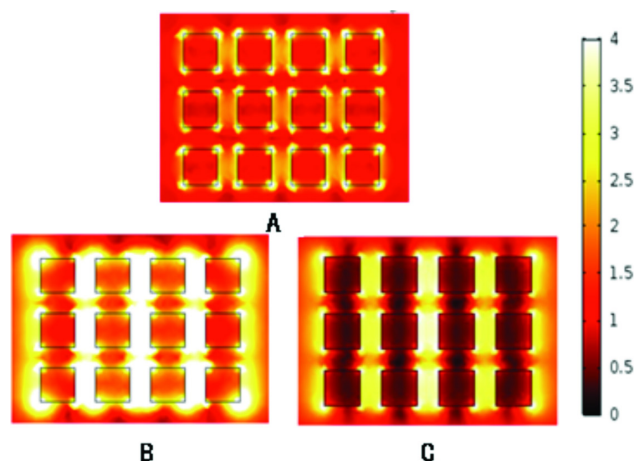
Insight into the working wavelength of hotspot effects generated by popular nanostructures

<https://doi.org/10.1515/ntrev-2019-0003>

Received Nov 22, 2018; accepted Dec 12, 2018

Abstract: A proper excitation wavelength is much important for the application of surface-enhanced Raman spectroscopy (SERS) in the biochemical field. Here, based on a SERS substrate model with an incident Gaussian beam, we investigate the dependence of the electric field enhancement on the incident wavelength of the excitation laser for popular nanostructures, including nanosphere dimer, nanorod dimer, and nanorod arrays. The results in the present manuscript indicate that both the nanosphere and nanorod dimer present a much broader plasmonic excitation wavelength range extending to the near-infrared region. The enhancement effect of Nanorod arrays is strongly dependent on the incident direction of excitation light. Finally, according to the conclusions above, a SERS substrate consisting of nanocubes based on the SPP eigenmode is proposed and the electric field enhancement is homogeneous, and insensitive to the polarization of the incident laser. The enhancement factor is not ultrahigh; however, good homogeneousness permits for quantitative detection of lower concentration components in mixtures.

Keywords: nanosphere dimer; nanorod dimer; nanorod arrays; hotspot; excitation wavelength



Graphical abstract: By investigating the dependence of the electric field enhancement on the incident wavelength of the excitation laser for popular nanostructures, we propose a SERS substrate consisting of Au nanocubes based on the SPP eigenmode. The electric field enhancement is homogeneous, and insensitive to the polarization of the incident laser. Though the enhancement factor is not ultrahigh, good homogeneousness permits for quantitative detection of lower concentration components in mixtures.

1 Introduction

Surface-enhanced Raman scattering (SERS) is a technique that enhances Raman signal as much as 10^{10} – 10^{11} by adsorbing molecules of interest on specific noble metal nanostructures. Therefore, various SERS substrates have been developed for the biochemical detection and imaging in recent years. Nanoparticles such as nanospheres [1], nanorods [2], and nanoshells [3] are the most popular nanostructures used as SERS substrates. Nanoparticle dimers are also proposed for SERS application because they have a much greater enhancement factor than single nanoparticles [4–6] (greater than 10^{10}). SERS phenomenon could be explained by plasmon resonance [7] (electromagnetic enhancement mechanism) or charge transfer resonance (chemical enhancement mechanism) [8, 9]. We give priority to the electromagnetic mechanism for designing specific metal nanostructure. The electromagnetic mechanism can also provide us quantitative explanations for unexpected SERS spectral changes. As we

*Corresponding Author: Yuee Li: School of Information Science and Engineering, Lanzhou University, Lanzhou 730000, China; Email: liyuee@lzu.edu.cn

*Corresponding Author: Qingguo Zhou: School of Information Science and Engineering, Lanzhou University, Lanzhou 730000, China; Email: zhouqg@lzu.edu.cn

Zhong Wang, Kesu Cai, Yang Lu, Haining Wu: School of Information Science and Engineering, Lanzhou University, Lanzhou 730000, China

know, surface plasmon polaritons are excited when the incident laser wavelength overlaps with the extinction spectrum of nanostructures. Hence, the electric field around the nano-particle is enhanced significantly and the radiation intensity that passes through the nanostructure suspension solution decreases. Therefore, optical properties of nanoparticles were inspected by analyzing UV-vis spectra at all times [10]. However, what is the electric field like when the laser beam is focused on these nanostructures, and how are the electric field distribution and enhancement related to the excitation wavelength? Recent studies show that the effect of SERS on nanorod arrays are strongly dependent on the polarization and angle of the incident laser [11]. However, the connection between the excitation wavelength and the structure size has not been systematically explored for optimization of SERS detection sensitivity. In some conditions, the selection of the excitation laser wavelength is still bewildering, especially for chemists and biologists.

Most commercial lasers possess linear polarization, the electric field of the optical wave possessing a variable magnitude but a constant direction along a straight line perpendicular to the direction of the wave. Here, we build an active electronicmagnetic model with the incidence of linear polarization Gaussian optical beam and study the relationship between the working wavelength and the enhancement factor of popular hotspot structures, including nanosphere dimer, nanorod dimers, and nanorod arrays distributed on a plane. In the last section of this paper, we propose a novel uniform SERS substrate, which is easy to fabricate. We evaluate the detection limit, homogeneity and stability of the enhancement along with its insensitivity to polarization (Figure S1 and Figure S2 in supplementary materials).

2 Results and Discussions

2.1 Nanosphere Dimer

Nanosphere dimer is experimentally verified to have strong near-field enhancement, and it has been applied to SERS detection [12, 13] and imaging [14–16]. Chemists and biologists have found it useful for various applications in the biochemical field. At the same time, it is also a basic unit of the nano cluster system. Therefore, it would be of great significance to explore the characteristics of Nanosphere dimer upon the excitation laser with varying wavelengths, polarization, and incident direction. In 2009, Xia prepared dimers of silver nanospheres and ex-

plored experimentally the influence of the laser polarization on SERS effects and observed a wider working wavelength compared with single silver sphere [12]. In 2011, Blaber applied gold nanosphere dimers for SERS in the infrared region [17]. Here, to fully examine the wavelength dependence characteristics, we calculated the electric field distribution of an Au nanosphere dimer with the radius 50nm and varying top-to-top distance D (3nm, 5nm, 10nm, 20nm) upon an incident linear polarization light ($E = E_y(x, y) e_y$, as shown in Figure 1(A)). The surrounded medium is considered as a water solution with the refractive index $n=1.4$. The experimental permittivity values of Au [18], varying with the working wavelength, were used for our calculation. Different from the single nanosphere, the hotspot effect is witnessed while the Gaussian beam is incident on the nanosphere dimer. The electric field around two nanospheres is similar to that of a single nanosphere while D is relatively large. However, a coupling of plasmon resonance between two nanospheres occurs, and the hotspot effects progressively enhance with the shrinkage of the gap (shown in Figure 1(B)).

The enhancement factor (EF) of SERS can be estimated by the following formula [19]

$$EF = \left| \frac{E_{loc}}{E_0} \right|^4$$

Where, $|E_0| = 1\text{V/m}$ is the modulus of incident field and E_{loc} is the local electric field distribution on SERS substrate. Here, we calculated $\left| \frac{E_{max}}{E_0} \right|^4$ for evaluation of SERS enhancement. $|E_{max}|$ is the maximum electric field on the straight line connecting the centers of the spheres and the relative value $\left| \frac{E_{max}}{E_0} \right|$ is shown in Figure 1(C). Notably, in contrast to a single nanosphere, the nanosphere dimer presents high near-field enhancement upon much broader excitation wavelengths extending to the near-IR, which is friendly to biological samples because of its low photon energy. This localized near-field energy shift can be considered a direct consequence of the damped, driven harmonic oscillators [20].

2.2 Nanorods Structures

Nanorods are still common nanostructures for constructing SERS tags because a single nanorod demonstrates a much broader surface plasmon resonance band than a single Nanosphere, extending to near-infrared wavelength [21]. Except for single nanorods, ordered Au nanorods arrays have also been developed as SERS substrates that produce a reproducible and strong SERS signal [22, 23]. Researchers further developed a gecko-

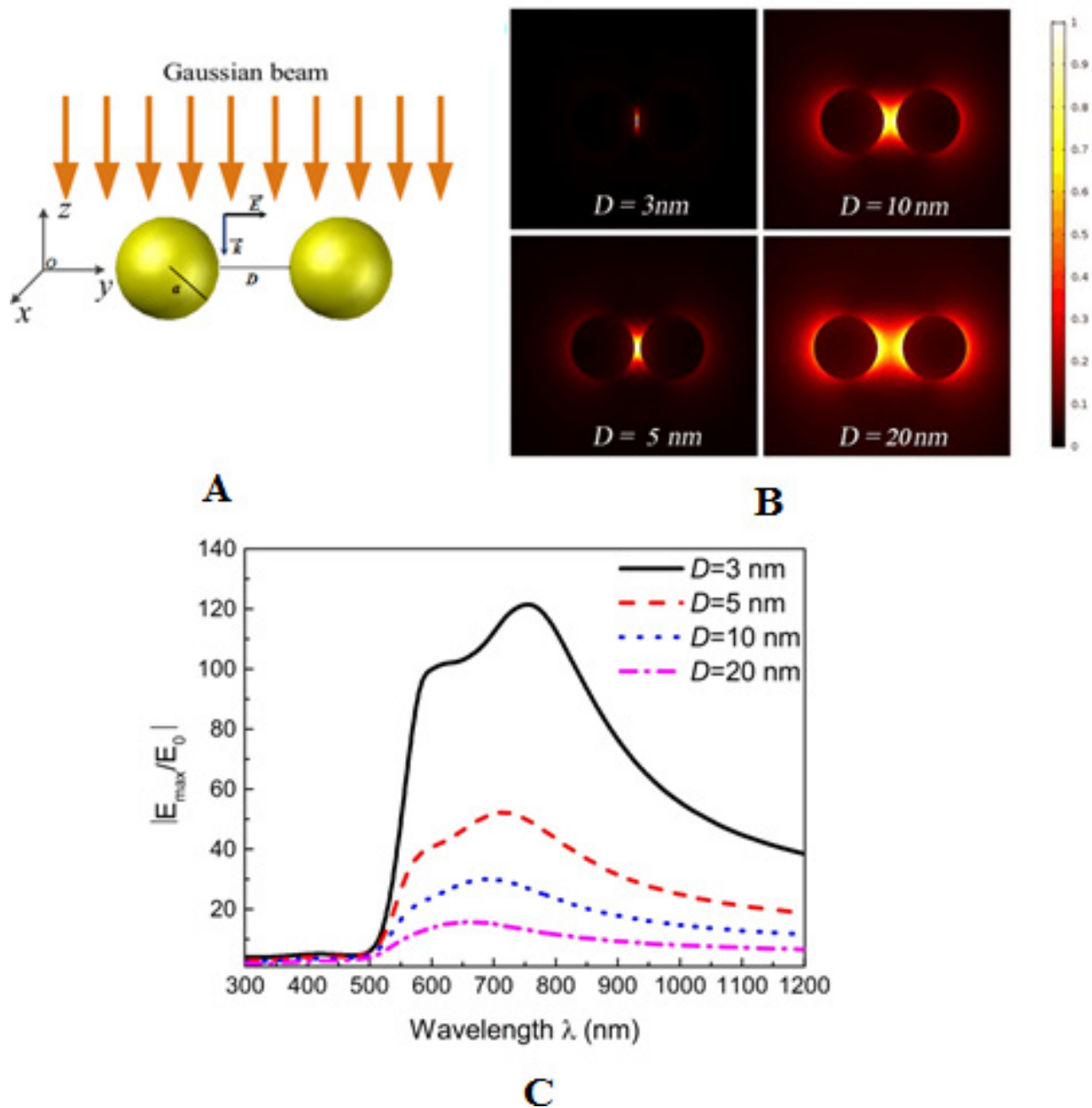


Figure 1: (A) Schematic diagram for the Gaussian beam incident on Au nanosphere dimer in the rectangular coordinate system; (B) The electric field distribution ($|E|$) around Au nanosphere dimer excited by incident Gaussian beam at $\lambda_0 = 633\text{ nm}$; (C) The curve of $|E_{\text{max}}/E_0|$ with the working wavelength ($|E_{\text{max}}|$ is the maximum electric field on the straight line connecting the centers of the spheres, $|E_0| = 1\text{ V/m}$ is the amplitude of the incident Gaussian beam)

inspired SERS platform composed of poly dimethylsiloxane nanorod arrays covered by silver nanoparticles [24]. For all those SERS structures, the wavelength and polarization orientation of the excitation light is very important for plasmon-induced electric field enhancement [25, 26].

The excitation laser can be incident on nanorod arrays from the longitudinal direction (Figure 2(A)) or the side direction (Figure 2(B)). Nanorod arrays are composed of numerous nanorod dimers, so we first analyze the nanorod

dimer. Here, to fully examine the wavelength dependence characteristics, we calculated the electric field distribution of an Au nanorod dimer with the radius $a = 50\text{ nm}$, height $h = 2a = 100\text{ nm}$ and varying top-to-top distance D (3 nm, 5 nm, 10 nm, 20 nm). The surrounded medium is considered as a water solution with the refractive index $n = 1.4$. In both incident cases, we set the polarization of the incident light as y direction to keep it in line with the dimer mode electric field. If the incident light is polarized along

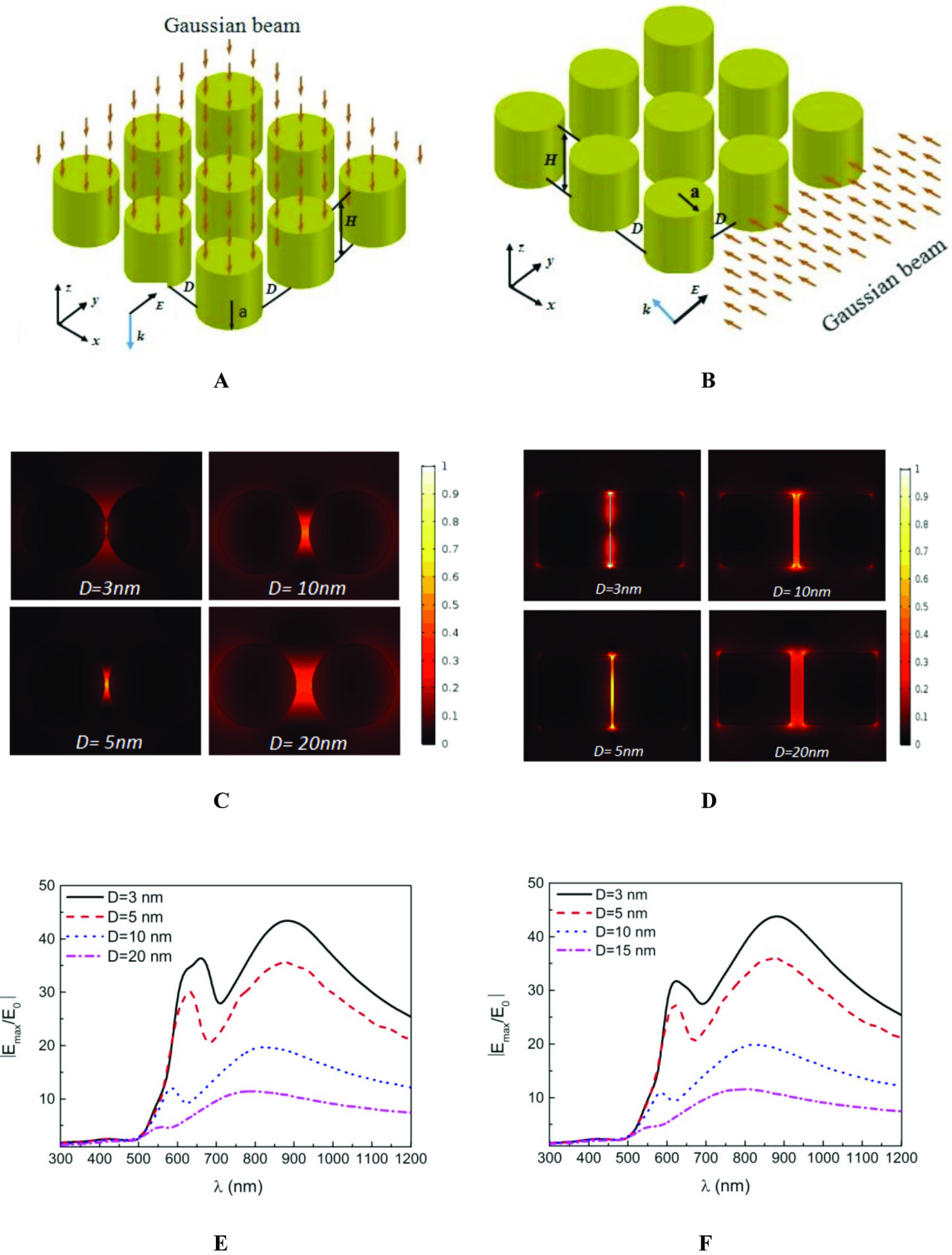


Figure 2: (A) Schematic diagram for the Gaussian beam incident on Au nanorod arrays from the longitudinal direction; (B) Schematic diagram for the Gaussian beam incident on Au nanorod arrays from the side direction; (C) Electric field distribution ($|E|$) around the Au nanorod dimer on the x-y section with the Gaussian beam longitudinal incident ($\lambda_0 = 633\text{ nm}$); (D) Electric field distribution ($|E|$) around Au nanorod dimer on y-z section with the Gaussian beam side incident ($\lambda_0 = 633\text{ nm}$); (E) The curve of $|E_{\max}/E_0|$ with the working wavelength for longitudinal incidence; (F) The curve of $|E_{\max}/E_0|$ with the working wavelength for side incidence; ($|E_{\max}|$ is the maximum electric field on the plane formed by the long axis of two nanorods, $|E_0|=1\text{ V/m}$ is the amplitude of the incident Gaussian beam)

z or x direction, the hotspot will not be excited. The maximum electric field $|E_{\max}|$ on the plane formed by the long axis of two nanorods are calculated and the relative value $\left|\frac{E_{\max}}{E_0}\right|$ (E_0 is the amplitude of the incident field) is shown in Figure 2(C). Our analyses show that the hotspot can be excited between two nanorods whether the light is incident from the longitudinal or the side direction (Figure 2(C) and (D)). The nanorod dimer shows a similar phenomenon in which the hotspot electric field becomes stronger while the gap distance declines and disappears while the gap is over $\sim 40\text{nm}$. In addition, the hotspot plasmonic effect works in broader wavelength ranges than that of the single nanorod (Figure 2(E) and (F)). Notably, the dependence of the enhancement factor on the wavelength shows the same variation for both incidence cases, which is acceptable because the plasmon resonance wavelength is commonly determined by the structure parameters of the SERS substrate. This wavelength dependence in Figure 2(E) and (F) also applies to nanorod arrays, but it is necessary to explore the electric field distribution for both incidence cases. As shown in Figure 3, the results indicate that the side excitation should be carefully used for SERS detection because the plasmonic field is getting weaker along with the incident direction, and consequently, the enhancement efficiency is significantly decreased.

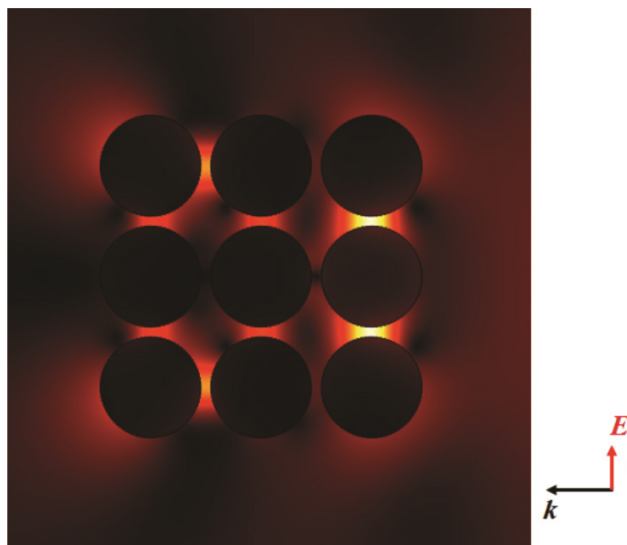


Figure 3: Electric field distribution ($|E|$) of Au nanorod arrays with a side incident Gaussian beam

2.3 Our Designed Structure and Application

The nanogap SPPs waveguide presents strong mode confinement and relative long propagation distance and the SPPs mode can be excited while the incident field owns the same direction with the electric field of eigenmode. Here, we propose a SERS substrate based on the concept of SPPs waveguide eigenmode. The substrate is composed of Au nanocube arrays and could be fabricated by electron beam lithography. It shows strong and homogeneous electric field enhancement while the linear polarization light is vertically incident on it. The schematic diagram for the Gaussian beam incident on this structure is given in Figure 4(A). Upon the working wavelength ranging from 300nm to 800nm, the electric field enhancement factor $\left|\frac{E_{\max}}{E_0}\right|$ has been analyzed for fixed side length of nanocube $a=50\text{nm}$ and varying gap $D=10\text{nm}$, 30nm, 50nm (Figure 4(B)).

In a broad range of visible light and the near-infrared region, our substrate shows good enhancement. Importantly, the hotspot presents a large area, accounting for half of the total substrate area, which leads to a much better average electric enhancement factor (Figure 4(C)).

We also calculated the electric field distribution on the x-y section of our designed structure ($a=50\text{nm}$ and $D=30\text{nm}$) at three excitation wavelengths 532nm, 633nm and 785nm, as shown in Figure 5. The water solution with the refractive index $n=1.4$ is considered as the surrounded material. The hotspot effects of this structure are strongly dependent on the excitation wavelength, and the electric field in the gap of nanocube reaches the maximum at 633nm, which is consistent with the wavelength dependence curve (red dash line) in Figure 4(B). To inspect the performance of this substrate, we fabricated this structure by electron beam lithography and detect crystal violet with low concentration on the spontaneous Raman system with 532nm laser excitation. The results indicate that the fluorescent background from crystal violet is significantly quenched by this substrate; the Raman signal with excellent SNR is acquired and the detection limit is as low as 10^{-7} M (Figure 6(C)). Furthermore, we mapped a $10\mu\text{m}\times 10\mu\text{m}$ area to acquire the Raman spectra from distributed points on our substrates, the intensity shows few changes and a few spots are caused by slight variation of SERS signal (Figure 6(C)). Due to the limitation of our equipment, we didn't perform our experiments on more excitation wavelengths though we believe that the higher detection limit could be achieved at 633nm excitation. It is commonly used for Raman signal excitation in the biological detection field. In the future work, we will develop 633nm Raman system and apply our substrates for spe-

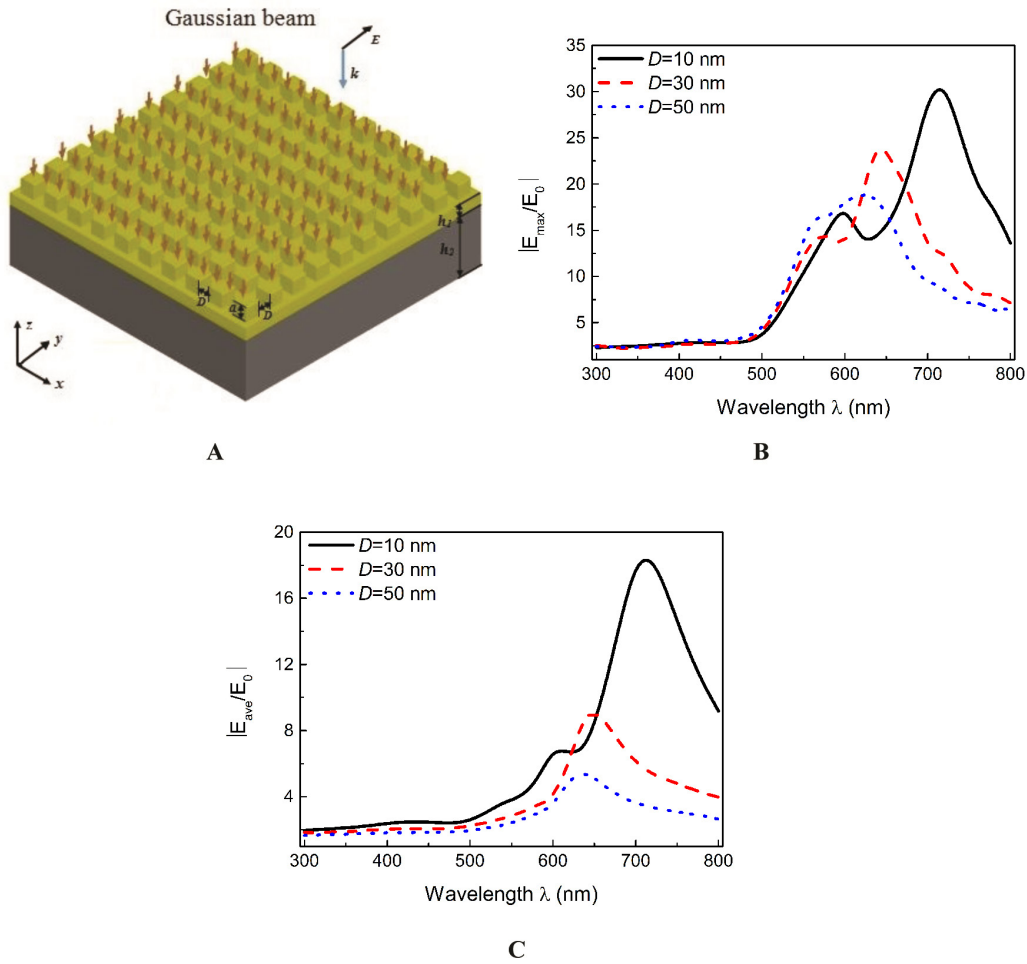


Figure 4: (A) Schematic diagram for the Gaussian beam incident on Au nanocube arrays; (B) The curve of $|E_{\max}/E_0|$ with the working wavelength; (C) The curve of $|E_{\text{ave}}/E_0|$ with the working wavelength ($|E_{\max}|$ is the maximum electric field in the space area; $|E_0| = 1\text{V/m}$ is the amplitude of the incident Gaussian beam; $|E_{\text{ave}}|$ is obtained by averaging $|E|$ in the whole space area)

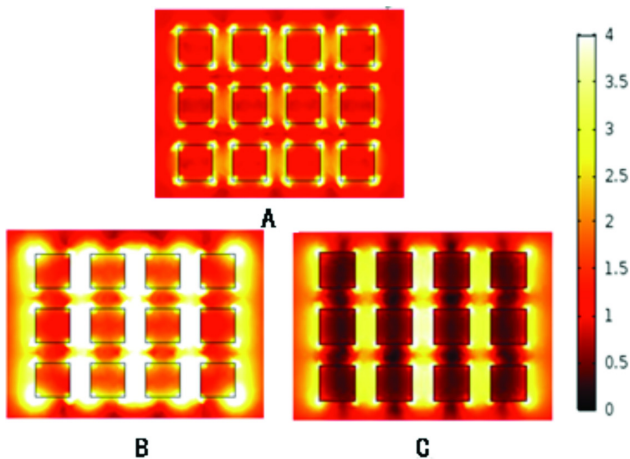


Figure 5: Electric field distribution on the x-y section with $D=30\text{nm}$ at: (A) $\lambda_0 = 532\text{nm}$; (B) $\lambda_0 = 633\text{nm}$; (C) $\lambda_0 = 785\text{nm}$

cific detection in biological field such as cell and tissue. Particularly worth mentioning is that, the molecular adsorption on plasmonic nanostructures and the interaction between adsorbed molecules and enhanced electric-field play a great role for the SERS signal of specific components.

2.4 Experimental Section

Sample preparation:

PMMA was spanned at 3000 rpm on the SiO_2/Si wafer using 5% 950 K PMMA solution in MIBK. The PMMA-coated wafer is annealed at 175°C for 90 min. The e-beam vector-scan system with a 30 nm beam size is used for fabrication. After exposure, the pattern is developed in a 1:3 mixture of MIBK and isopropanol at 21.2°C . The Au cube arrays are

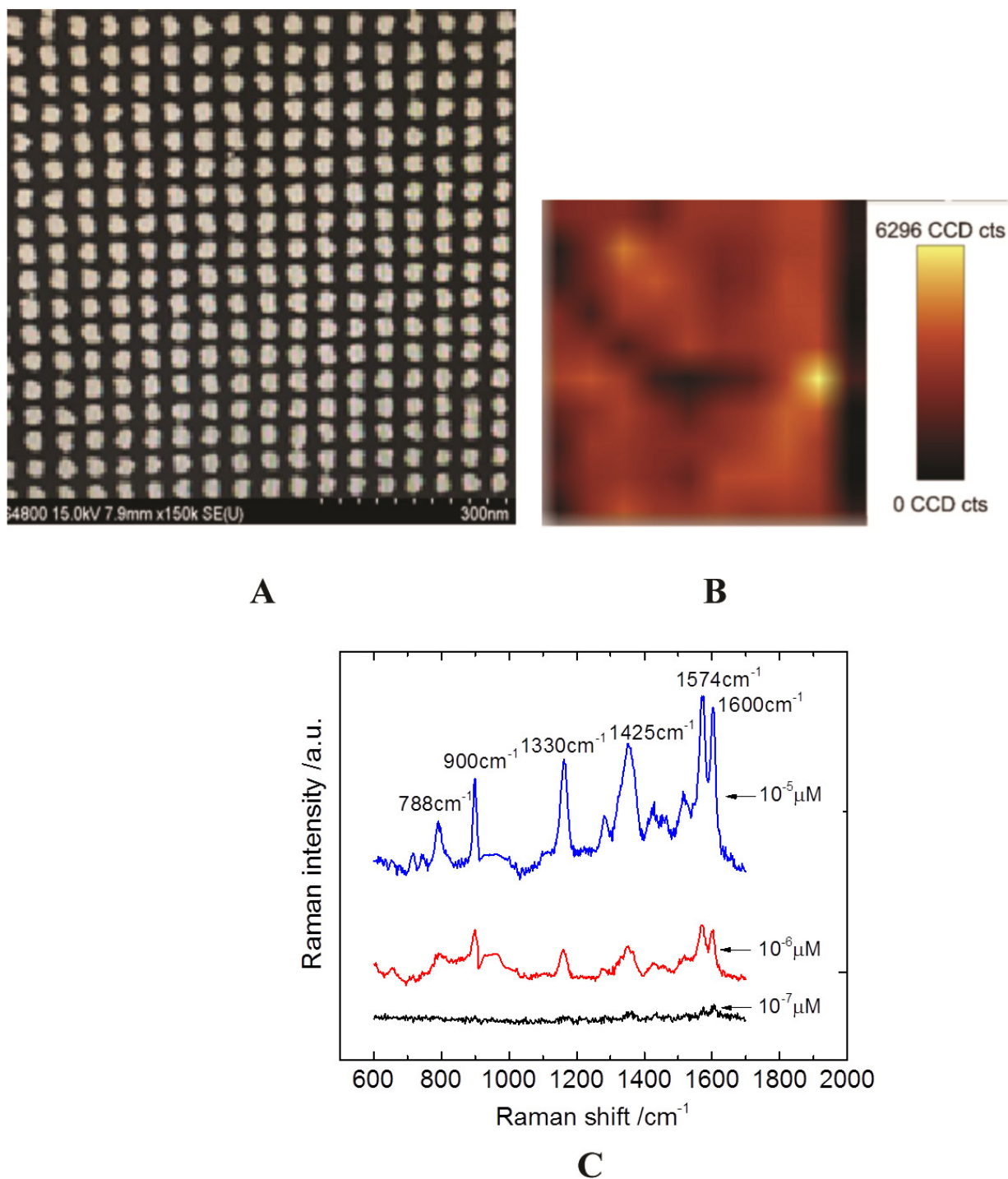


Figure 6: (A) Top-view SEM image of our nanocube arrays substrate; (B) mapping of SERS signals (1330cm^{-1}) at a $10\mu\text{m}\times 10\mu\text{m}$ substrate area with $10\mu\text{M}$ Crystal Violet concentration; (C) SERS signals of crystal violet enhanced by our SERS substrate with concentrations 10^{-5} , 10^{-6} and 10^{-7} M (Laser wavelength: 532nm , Power: 3mW , Accumulation time: 1s)

produced by e-beam evaporation of 5nm Ti and 45nm Au using the developed patterns as a template. Our SERS substrate is obtained after the lift-off process in hot acetone $\sim 90^\circ\text{C}$. Crystal Violet (Amresco0528) was purchased from Amresco. The substrate is cleaned out before usage. $1\mu\text{L}$

water solutions of Crystal Violet with $10^{-5}\mu\text{M}$, $10^{-6}\mu\text{M}$ and $10^{-7}\mu\text{M}$ concentrations are allowed to stand for 2hs to ensure a thin layer coverage on the nanostructure.

Raman spectra measurement:

Raman spectroscopy was performed using Alpha 300R confocal Raman microscope system (WITec, Germany) equipped with 532 nm (Verdi V-6) as laser sources for excitation, and ACTON 300i spectrometer with Pixis Spec 10-100 CCD camera (Princeton Instruments, Trenton, NJ). The laser beam was focused into the sample by a Zeiss LD EC Epiplan-Neofluar 50x objective lens with NA 0.55 (Nikon, Japan).

Numerical calculation:

The characteristics and the electromagnetic field distributions of all nanostructures were calculated based on 3D FEM methods (COMSOL Multiphysics) with perfect matching boundary condition. In calculations, a linearly polarized Gaussian beam was used to illuminate the nanostructures and non-uniform meshes were employed to save computation time (the maximum mesh $\lambda_0/8$ and the minimum mesh 2nm is used for validity of our calculation). The dielectric function of gold was taken from a fitting model offered by COMSOL software. We considered the surrounded medium as the water solution with the refraction index $n=1.4$ for all nanostructures.

3 Conclusion

The present paper established an active model of SERS substrate and investigated the dependence of electric field enhancement on the excitation wavelength for several typical hotspot nanostructures based on this active model. The results are of great value for designing novel SERS substrate and selection of the excitation wavelength in SERS experiments. Furthermore, we proposed a nanotube array of SERS substrate with high SERS activity, stability, and reproducibility. This substrate is manufactured by electron beam lithography, its shape and spatial arrangement being finely controlled. The enhancement factor of our substrate is not as high as that of NS dimer with a small gap, but the SERS signal can be obtained over the whole sample surface, rather than at discrete points. In addition, we believe that further optimization of the electron beam lithography process will increase the electric field enhancement factor. In addition, this substrate has exhibited long-standing stability and can be used repeatedly after ultrasonic cleaning; hence, this substrate is more ap-

plicative for liquid bulk detection in the biological and chemical fields.

Acknowledgement: This work was supported by the National Natural Science Foundation of China (NSFC) (Grant Nos. 61405083), the Fundamental Research Funds for the Central Universities (Izujbky-2018-129), and the Natural Science Foundation of Gansu Province of China (Grant Nos. 17JR5RA197).

References

- [1] Sprague-Klein, E.A., M.O. McAnally, D.V. Zhdanov, A.B. Zrimsek, V.A. Apkarian, T. Seideman, G.C. Schatz, and R.P. Van Duyne, *Observation of Single Molecule Plasmon-Driven Electron Transfer in Isotopically Edited 4,4'-Bipyridine Gold Nanosphere Oligomers*. J Am Chem Soc, 2017. **139**(42): 15212-15221.
- [2] Zhan, P., P.K. Dutta, P. Wang, G. Song, M. Dai, S.X. Zhao, Z.G. Wang, P. Yin, W. Zhang, B. Ding, and Y. Ke, *Reconfigurable Three-Dimensional Gold Nanorod Plasmonic Nanostructures Organized on DNA Origami Tripod*. ACS Nano, 2017. **11**(2): 1172-1179.
- [3] Sun, D., Y. Tian, Y. Zhang, Z. Xu, M.Y. Sfeir, M. Cotlet, and O. Gang, *Light-Harvesting Nanoparticle Core-Shell Clusters with Controllable Optical Output*. ACS Nano, 2015. **9**(6): 5657-5665.
- [4] Tan, X.B., Z.Y. Wang, J. Yang, C.Y. Song, R.H. Zhang, and Y.P. Cui, *Polyvinylpyrrolidone- (PVP-) coated silver aggregates for high performance surface-enhanced Raman scattering in living cells*. Nanotechnology, 2009. **20**(44).
- [5] Huang, P.J., L.L. Tay, J. Tanha, S. Ryan, and L.K. Chau, *Single-Domain Antibody-Conjugated Nanoaggregate-Embedded Beads for Targeted Detection of Pathogenic Bacteria*. Chemistry-a European Journal, 2009. **15**(37): 9330-9334.
- [6] Huang, P.J., L.K. Chau, T.S. Yang, L.L. Tay, and T.T. Lin, *Nanoaggregate-Embedded Beads as Novel Raman Labels for Biodetection*. Advanced Functional Materials, 2009. **19**(2): 242-248.
- [7] Itoh, T., Y.S. Yamamoto, and Y. Ozaki, *Plasmon-enhanced spectroscopy of absorption and spontaneous emissions explained using cavity quantum optics*. Chem Soc Rev, 2017. **46**(13): 3904-3921.
- [8] Yamamoto, Y.S. and T. Itoh, *Why and how do the shapes of surface-enhanced Raman scattering spectra change? Recent progress from mechanistic studies*. Journal of Raman Spectroscopy, 2016. **47**(1): 78-88.
- [9] Yamamoto, Y.S., Y. Ozaki, and T. Itoh, *Recent progress and frontiers in the electromagnetic mechanism of surface-enhanced Raman scattering*. Journal of Photochemistry and Photobiology C: Photochemistry Reviews, 2014. **21**: 81-104.
- [10] Song, C., Z. Wang, R. Zhang, J. Yang, X. Tan, and Y. Cui, *Highly sensitive immunoassay based on Raman reporter-labeled immuno-Au aggregates and SERS-active immune substrate*. Biosens Bioelectron, 2009. **25**(4): 826-831.
- [11] Subr, M., M. Petr, O. Kylian, J. Stepanek, M. Veis, and M. Prochazka, *Anisotropic Optical Response of Silver Nanorod Arrays: Surface Enhanced Raman Scattering Polarization and Angu-*

- lar Dependences Confronted with Ellipsometric Parameters. Sci Rep, 2017. **7**(1): 4293.
- [12] Li, W., P.H. Camargo, X. Lu, and Y. Xia, *Dimers of silver nanospheres: facile synthesis and their use as hot spots for surface-enhanced Raman scattering*. Nano Lett, 2009. **9**(1): 485-490.
- [13] Li, W., P.H. Camargo, L. Au, Q. Zhang, M. Rycenga, and Y. Xia, *Etching and dimerization: a simple and versatile route to dimers of silver nanospheres with a range of sizes*. Angew Chem Int Ed Engl, 2010. **49**(1): 164-168.
- [14] Lim, D.K., K.S. Jeon, H.M. Kim, J.M. Nam, and Y.D. Suh, *Nanogap-engineerable Raman-active nanodumbbells for single-molecule detection*. Nat Mater, 2010. **9**(1): 60-67.
- [15] Cong, V.T., N.H. Ly, S.J. Son, J. Min, and S.W. Joo, *Silica-encapsulated gold nanoparticle dimers for organelle-targeted cellular delivery*. Chem Commun (Camb), 2017. **53**(36): 5009-5012.
- [16] Lu, H., L. Zhu, C. Zhang, K. Chen, and Y. Cui, *Mixing Assisted "Hot Spots" Occupying SERS Strategy for Highly Sensitive In Situ Study*. Analytical Chemistry, 2018.
- [17] Blaber, M.G. and G.C. Schatz, *Extending SERS into the infrared with gold nanosphere dimers*. Chemical communications (Cambridge, England), 2011. **47**(13): 3769-3771.
- [18] Johnson, P.B. and R.W. Christy, *Optical Constants of the Noble Metals*. Physical Review B, 1972. **6**(12): 4370-4379.
- [19] Le Ru, E.C., P.G. Etchegoin, and ebrary Inc., *Principles of surface-enhanced Raman spectroscopy and related plasmonic effects*. 2009, Elsevier: Amsterdam ; Boston. p. xxiii, 663 p.
- [20] Zuloaga, J. and P. Nordlander, *On the Energy Shift between Near-Field and Far-Field Peak Intensities in Localized Plasmon Systems*. Nano Lett, 2011. **11**(3): 1280-1283.
- [21] Wang, Y., Y. Wang, W. Wang, K. Sun, and L. Chen, *Reporter-Embedded SERS Tags from Gold Nanorod Seeds: Selective Immobilization of Reporter Molecules at the Tip of Nanorods*. ACS Appl Mater Interfaces, 2016.
- [22] Huang, Z., G. Meng, B. Chen, C. Zhu, F. Han, X. Hu, and X. Wang, *Surface-Enhanced Raman Scattering from Au-Nanorod Arrays with Sub-5-nm Gaps Stuck Out of an AAO Template*. J Nanosci Nanotechnol, 2016. **16**(1): 934-938.
- [23] De, R., Y.S. Shin, C.L. Lee, and M.K. Oh, *Long-Standing Stability of Silver Nanorod Array Substrates Functionalized Using a Series of Thiols for a SERS-Based Sensing Application*. Appl Spectrosc, 2016. **70**(7): 1137-1149.
- [24] Wang, P., L. Wu, Z. Lu, Q. Li, W. Yin, F. Ding, and H. Han, *Gecko-Inspired Nanotentacle Surface-Enhanced Raman Spectroscopy Substrate for Sampling and Reliable Detection of Pesticide Residues in Fruits and Vegetables*. Anal Chem, 2017. **89**(4): 2424-2431.
- [25] Ming, T., L. Zhao, Z. Yang, H. Chen, L. Sun, J. Wang, and C. Yan, *Strong Polarization Dependence of Plasmon-Enhanced Fluorescence on Single Gold Nanorods*. Nano Lett, 2009. **9**(11): 3896-3903.
- [26] Zhang, M., C. Li, C. Wang, C. Zhang, Z. Wang, Q. Han, and H. Zheng, *Polarization dependence of plasmon enhanced fluorescence on Au nanorod array*. Appl Opt, 2017. **56**(3): 375-379.

Supplementary information

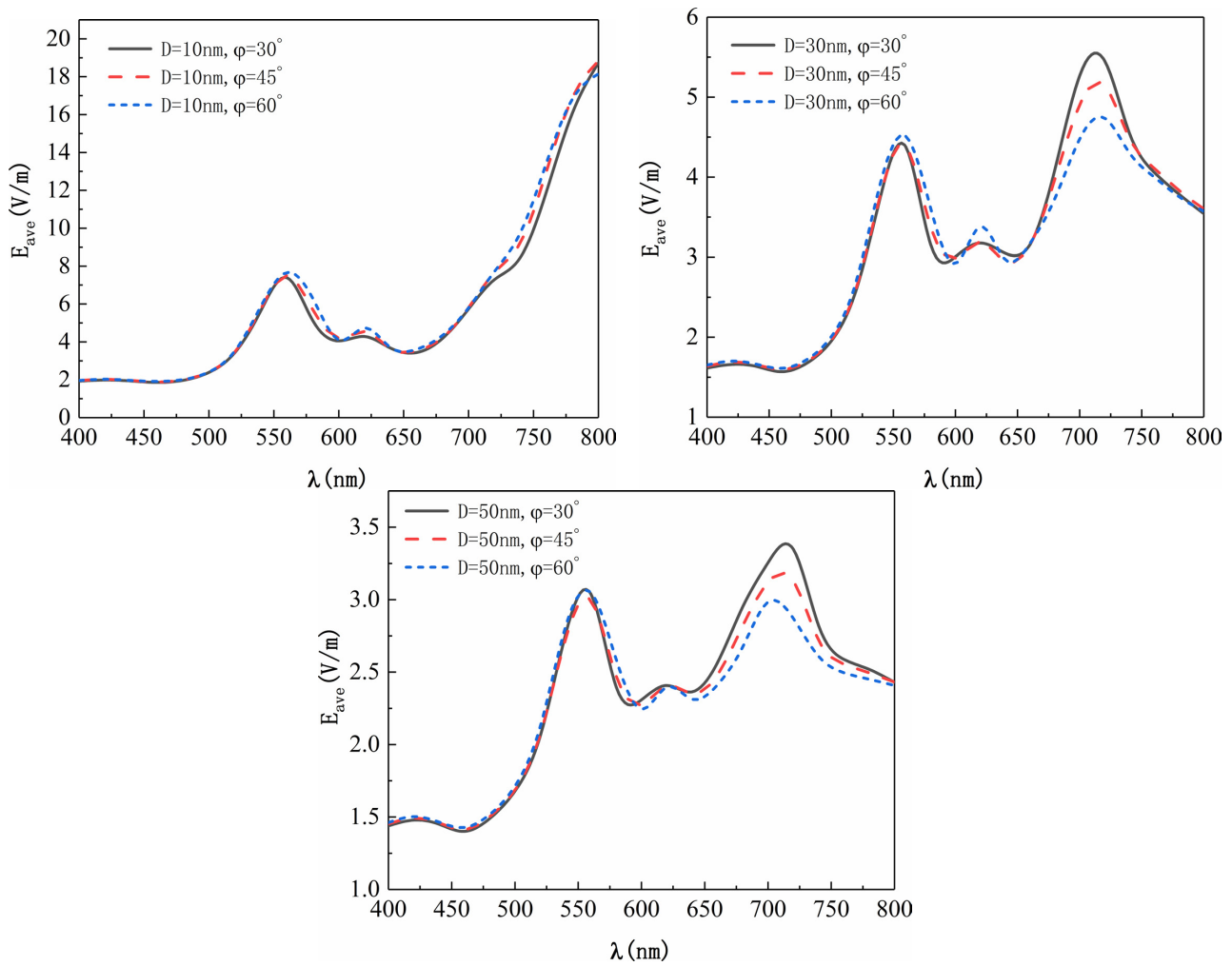


Figure S1: Curve of average electric field enhancement with the working wavelength (E_0 is the amplitude of the incident Gaussian beam; $|E_{ave}|$ is obtained by averaging $|E|$ in the whole space area)

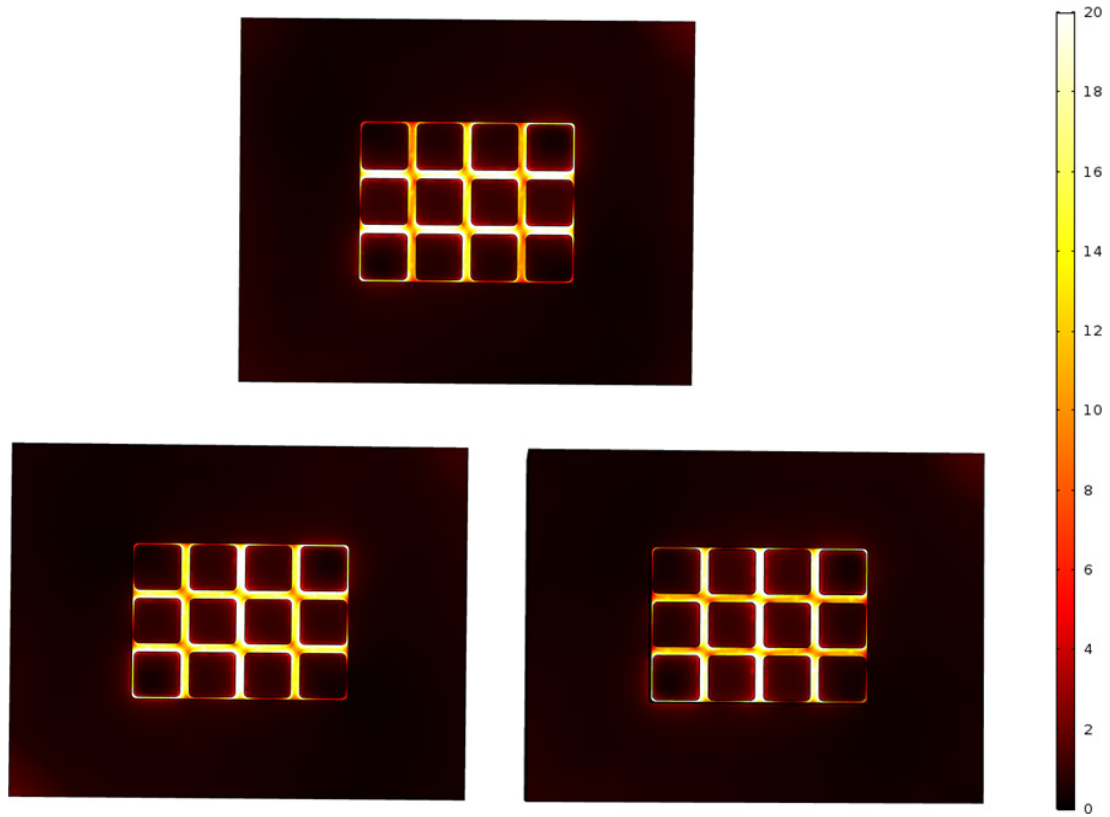


Figure S2: Electric field distribution on the x-y section with $D=30\text{nm}$ and various polarization: (a) $\frac{\pi}{6}$; (b) $\frac{\pi}{4}$; (c) $\frac{\pi}{3}$